



TIDAL EFFECTS ON CHANGJIANG PLUME DISPERSAL IN THE EAST CHINA SEA

Hung-Jen Lee

*Department of Marine Environmental Informatics, National Taiwan Ocean University, Keelung, Taiwan, R.O.C.,
lecgvyer@mail.ntou.edu.tw*

Kon-Kee Liu

Institute of Hydrological and Oceanic Sciences, National Central University, Jungli, Taiwan, R.O.C.

Follow this and additional works at: <https://jmst.ntou.edu.tw/journal>

Recommended Citation

Lee, Hung-Jen and Liu, Kon-Kee (2013) "TIDAL EFFECTS ON CHANGJIANG PLUME DISPERSAL IN THE EAST CHINA SEA," *Journal of Marine Science and Technology*. Vol. 21: Iss. 3, Article 13.

DOI: 10.6119/JMST-013-0207-1

Available at: <https://jmst.ntou.edu.tw/journal/vol21/iss3/13>

This Research Article is brought to you for free and open access by Journal of Marine Science and Technology. It has been accepted for inclusion in Journal of Marine Science and Technology by an authorized editor of Journal of Marine Science and Technology.

TIDAL EFFECTS ON CHANGJIANG PLUME DISPERSAL IN THE EAST CHINA SEA

Acknowledgements

We are especially grateful for the kind help of C.-K. Hu (TORI) and S. Jan (IONTU). Author HJL was sponsored by the National Science Council (Taiwan) under grants NSC100-2611-M-019-003.

TIDAL EFFECTS ON CHANGJIANG PLUME DISPERSAL IN THE EAST CHINA SEA

Hung-Jen Lee¹ and Kon-Kee Liu²

Key words: Changjiang River plume, tidal currents, wind-driven currents.

ABSTRACT

We incorporated tidal currents into a previously validated three-dimensional subtidal circulation model, and used it to assess the manner in which tides affect the Changjiang plume dispersal. The coupled model results show that competition in both tidal and wind-driven currents occurs during the winter season. However, the northeasterly winds are predominant in the competition because they transport large amounts of brackish water to the south along the southeastern China coast. In general, the summer tidal currents disperse Changjiang plume more southward and seaward rather than northward for the case without tides; however, the winter tidal currents seem to reduce their effects. In winter, the tidal currents may cause strong turbulent tidal mixing with their ambient water, particularly close to the coastal boundaries. Thus, results more closely aligned with observations of Changjiang River plumes were obtained from the tide-circulated coupling model than from the general circulation model.

I. INTRODUCTION

The East China, Yellow, and Bohai Seas (the so-called three-sea system) are interconnected and form large shallow-water marginal seas in the northwestern Pacific Ocean. Among the three seas (East China Sea, Yellow Sea, and Bohai Sea) extending from 25 to 41°N (Fig. 1), the largest sea (East China Sea) is sufficiently open to the western Pacific Ocean. Shoreward of the Kuroshio, the northward Taiwan Warm Current (TWC) enters the East China Sea (ECS) from the Taiwan Strait [1]. By contrast, the Yellow Sea (YS) and Bohai Sea (BS) do not have major currents to drive their circulation. The mouth or estuary of the Changjiang River is far away from the

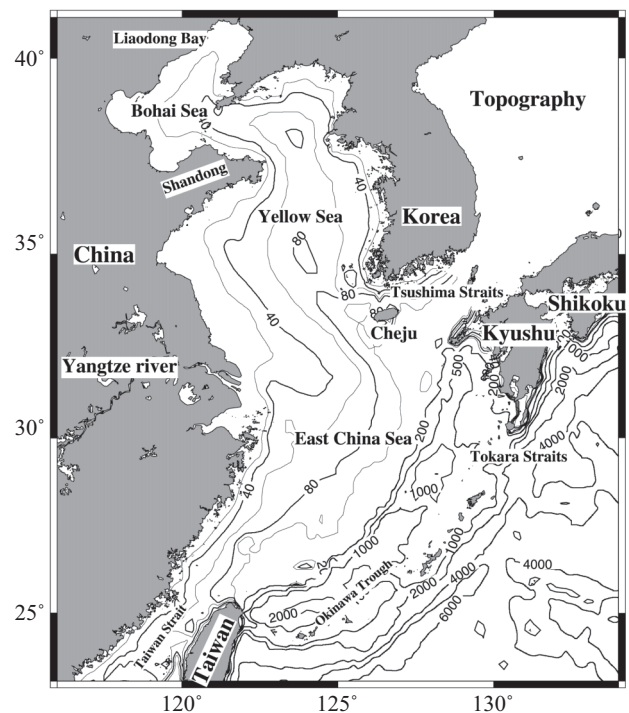


Fig. 1. Model domain and isobaths (in meters) of the East China Sea and surroundings excluding the Sea of Japan.

main stream of the Kuroshio, at least more than 500 km, and its circulation is infrequently affected by the Kuroshio. Previous studies [3, 9, 13, 19] bear out the foregoing conclusion.

In addition to boundary currents, the East Asia monsoon efficiently drives seasonal circulation in the three-sea system. Fig. 2, derived from NCEP data, shows the climatologic wind-stress fields in August and December. Over the East China Sea, the prevailing winds are mostly southerly-southeasterly from July to mid-September, and subsequently changes to northerly-northeasterly until April of the following year [16]. Over the Yellow and Bohai Seas, the monsoon winds generally weaken with distance from the East China Sea.

Because light freshwater from a river debouches into saline water in the estuary, the behavior of river plumes is usually influenced by a number of factors, including the earth rotating effect, estuary-shelf topography, river discharge, subtidal currents, tidal forcing, and local winds. In a coupled estuary-shelf

Paper submitted 08/30/12; revised 01/25/13; accepted 02/07/13. Author for correspondence: Hung-Jen Lee (e-mail: lecgyver@mail.ntou.edu.tw).

¹ Department of Marine Environmental Informatics, National Taiwan Ocean University, Keelung, Taiwan, R.O.C.

² Institute of Hydrological and Oceanic Sciences, National Central University, Jungli, Taiwan, R.O.C.

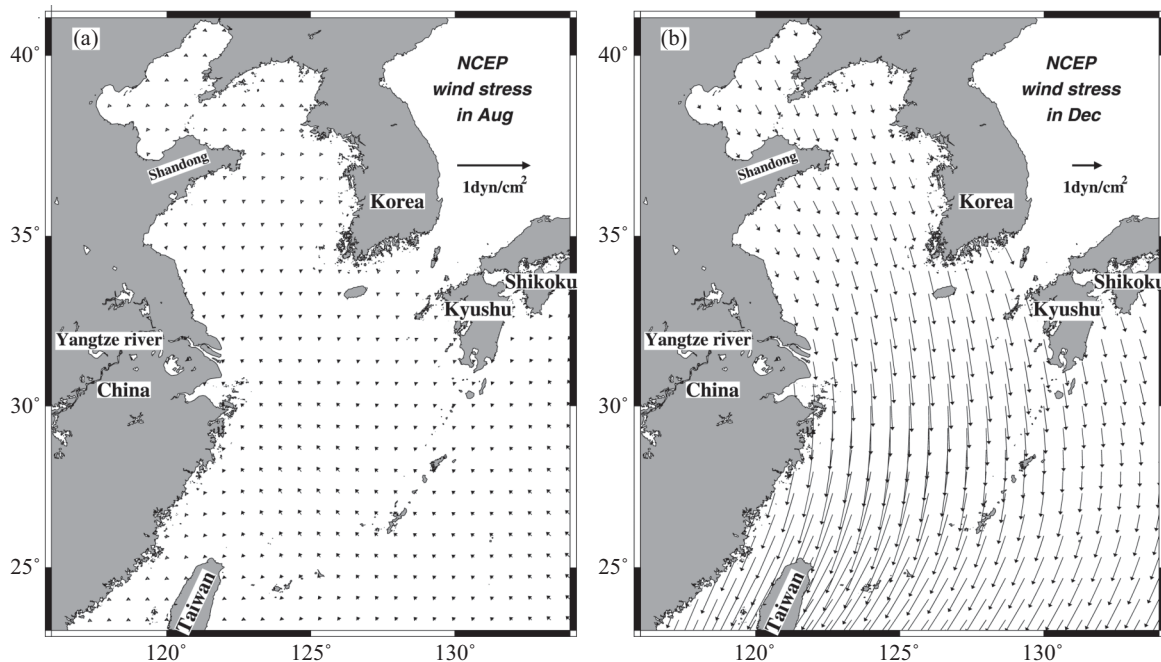


Fig. 2. Monthly climatologic wind stress fields derived from NCEP in (a) August and (b) December.

environment, winds, tides, and river discharge are the three main forces that support the system and drive the estuarine circulations [2]. In absence of wind, coastal subtidal flow, and tidal current situations, the rotational effect of the earth plays a crucial role in the behavior of river plumes for wide estuaries [3, 4]. A numerical circulating ocean model without tidal forcing had been conducted by Chao and Boicourt [4] using the Bryan-Cox-Semtner three-dimensional primitive equation model with various vertical diffusive/mixing coefficients. Chao and Boicourt [4] assumed that the simplified model was a rigid-lid and a flat bottom with a baroclinic flow. Chao and Boicourt indicated that the light freshwater flowing over saline water and into the estuary expands immediately when it leaves the river mouth and forms a bulge of anticyclonic surface flow. The plume following the flow anticyclonically turns to the right facing seaward, carrying light freshwater over a large distance to the downstream along the right-hand side coast. The Coriolis force is crucial for wide estuaries [4, 20, 26].

Changjiang, or the Yangtze River, is the main supplier of freshwater, sediments, and river-borne nutrients to the East China Sea [1, 15, 17]. Their subsequent dispersals occur under the influence of monsoon winds, the Taiwan Warm Current, the Kuroshio intrusion and the periodical tidal currents. Shoaling tidal currents and their spring-neap variations [11, 18, 24] regulate the freshwater discharge and subsequent mixing with surrounding seawater [1]. They also play a vital role in the seaward transport of Changjiang sediments [17].

Historical observed data have shown that light freshwater pouring into the estuary forms a thin layer plume and floats over more dense seawater. The interface between the thin layer of freshwater and the dense seawater easily occurs

slippery. Wu *et al.* [24] studied the Changjiang River plume using a three-dimensional numerical model with tides, and their results indicated the crucial role of tidal forcing in modulating the Changjiang River plume. They also indicated that, without tidal forcing, the plume results in an unrealistic phenomenon in the upstream extension.

Regarding numerical modeling, previous studies on Changjiang plume dispersal were fragmented. For example, Lee and Chao [9] included all major forces, except tides. It may be necessary to merge the two approaches including general circulation and tidal currents, and becomes a tide-circulated coupling numerical model. Therefore, this study incorporated tidal forcing into the subtidal model of Lee and Chao [9] and examined the consequences. In addition, we further attempted to understand the differences among seasons of the sea surface temperature (SST) and sea surface salinity (SSS) with and without tides in the three-sea system.

II. TIDAL AND SUBTIDAL CIRCULATION MODEL

The model solves 3-D temperature, salinity, and momentum equations under hydrostatic and Boussinesq approximations. The conservation equations for temperature (T) and salinity (S) are

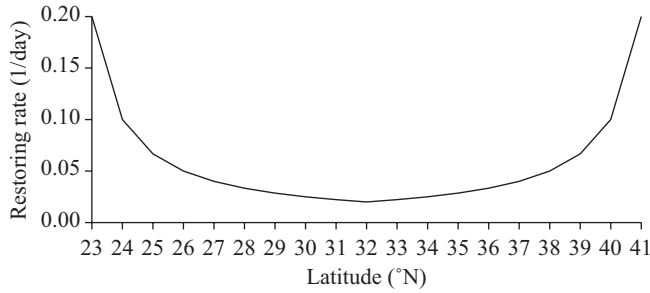
$$\partial_t T + \mathbf{v}\nabla T + w\partial_z T = \theta + r(T^* - T), \quad (1)$$

$$\partial_t S + \mathbf{v}\nabla S + w\partial_z S = \delta + r(S^* - S), \quad (2)$$

where θ and δ are mixing terms, \mathbf{v} is the horizontal velocity

Table 1. Monthly discharge (Sv), temperature (°C) and salinity (psu) for the Changjiang River inflow.

Month	Jan	Feb	Mar	Apr	May	Jun	Jul	Aug	Sep	Oct	Nov	Dec
Discharge	0.01	0.013	0.016	0.023	0.037	0.042	0.05	0.045	0.043	0.037	0.025	0.016
Temperature	8.0	9.0	12.0	14.0	18.0	22.0	25.0	25.0	23.0	18.0	14.0	10.0
Salinity	0.0	0.0	0.0	0.0	0.0	0.0	0.0	0.0	0.0	0.0	0.0	0.0

**Fig. 3. The varying restoration rate (day⁻¹) for temperature and salinity fields is dependent on the latitude in the top 30 m of the ocean.**

vector, and w is the vertical velocity. Following Sarmiento and Bryan [23], we nudge temperature and salinity slowly toward their respective climatologic values, T^* and S^* [12] with a latitude-dependent restoration rate (r). Its magnitude between 0 and 30 m is approximately $1/50 \text{ day}^{-1}$ at the latitude of 32°N , and increases towards the North and South directions from $1/50$ (32°N) to $1/10 \text{ day}^{-1}$ (23 or 41°N), as shown in Fig. 3. Moreover, the value of restoration rate is 0 between 30 and 150 m, and $1/15 \text{ day}^{-1}$ below 150 m. In the thermocline, this measure allows it to move freely. In addition, the nudging calculation becomes diagnostic if r is excessively large and prognostic if r is small. Because climatologic T^* and S^* with 1-degree resolution are excessively coarse to resolve the Changjiang plume, we use a smaller value of r to allow considerable deviations. To reduce erroneous water mass flux into the East China Sea, the freshwater is released at the upstream boundary of 5 grids up the Changjiang mouth. Under rigid-lid condition to eliminate surface gravity waves, which we had examined.

The study area extends from 23° to 41°N in latitude and 118° to 134°E in longitude with a horizontal resolution of $1/6^\circ$, and $\Delta x = \Delta y = 18.5 \text{ km}$ approximately; the total grids are 109 by 109 points in horizontal directions. In our 3-D model, Δt is 8 s for the barotropic mode and ΔT is 400 s for the baroclinic mode. Because both are smaller than the M_2 tidal period of 12.42 h, the model requires only calculation of the baroclinic set of equations once every fifty barotropic calculation. Excluding sea level variations, the top layer is 5 m thick on average. Beneath the top surface layer, the thickness of each layer is 85% that of the layers immediately below. Its maximal depth reaches 6018 m, and there are 33 levels in the vertical direction. The horizontal mixing coefficient is $5000 \text{ m}^2/\text{s}$ for momentum and $50 \text{ m}^2/\text{s}$ for temperature and salinity.

The coefficients of vertical viscosity and diffusivity are

calculated from the Richardson number according to the formulation of Pacanowski and Philander [21]. All solid boundaries are impermeable and non-slip, except at the bottom, where the quadratic bottom friction coefficient is 0.0015, the value of which is to better develop for the semidiurnal tide according to the suggestion of Guo and Yanagi [7]. Therefore, the value of the sea bed drag coefficient is adopted and fixed through all model runs in our study.

The monthly climatological wind stress (NCEP data, averaged from 1979 to 2006) is exerted at the sea surface (Fig. 2). Monthly mean inflows and outflows through open ocean boundaries are referred to Lee and Chao [9] for justifications. For the Changjiang discharge, Table 1 shows the monthly mean inflow, temperature, and salinity compiled by the Global Runoff Data Center of the Federal Institute of Hydrology in Germany [10].

In addition to mean currents, we also impose tidal currents on open boundaries using the result from a 2-D barotropic tide model with $1/12^\circ$ resolution [8]. Their tide-induced sea level contains 6 tidal constituents (P_1 , O_1 , K_1 , N_2 , M_2 and S_2),

$$\zeta = \sum_{n=1}^6 \zeta_n \cos(\omega_n t + \theta_n), \quad (3)$$

where ω_n is the frequency, ζ_n is the amplitude, and θ_n is the phase lag of tidal constituents. Our model year is climatologic in the sense that, in addition to using monthly climatologic forcing, each month contains 30 days. Unlike Guo and Yanagi [7] and Yanagi *et al.* [25], we did not simulate a real ocean or compared the modeled sea level with the corresponding observed sea-level data in detail because this was beyond our scope. Our model was used to understand tidal forcings that affect SST and SSS fields rather than improve tidal predictions.

Assuming linearity [5, 22], the corresponding tidal currents are

$$\mathbf{V}_{\text{tidal current}} = (g/D)^{1/2} \sum_{n=1}^6 \zeta_n \cos(\omega_n t + \theta_n), \quad (4)$$

where D is the undisturbed water depth on open boundaries and g is the gravitational acceleration.

Hence, the water flow of the 3-D model penetrating each open boundary is concurrently driven by the monthly mean currents and the tidal currents, described as follows:

$$\mathbf{V}_{\text{normal}} = \mathbf{V}_{\text{monthly mean current}} + \mathbf{V}_{\text{tidal current}}$$

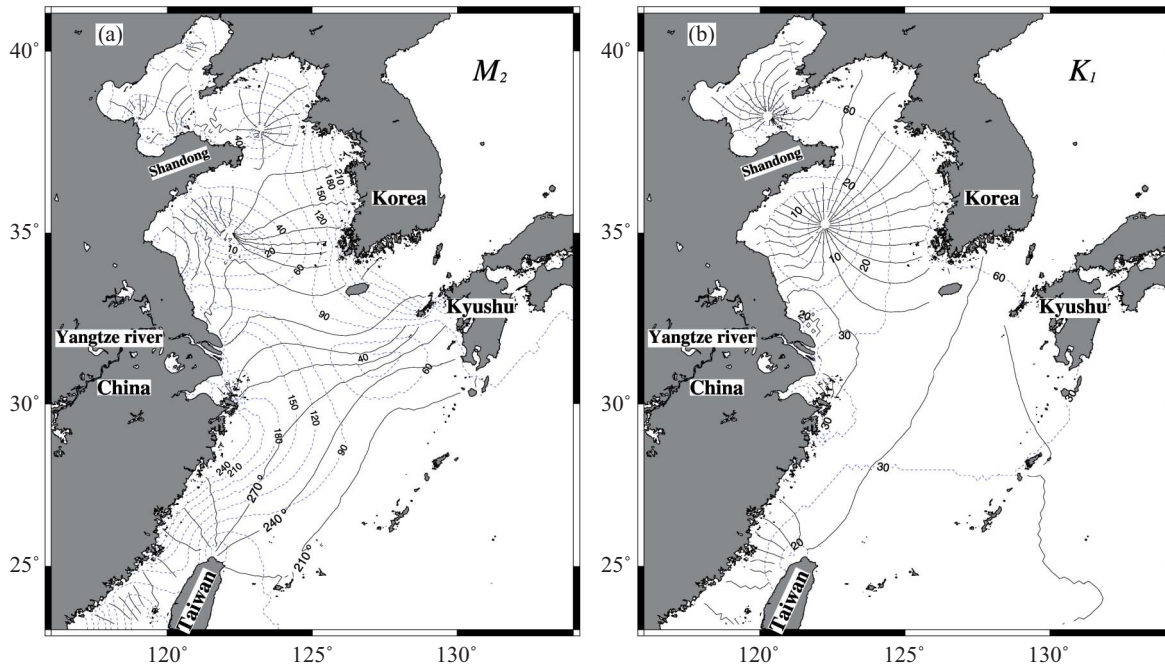


Fig. 4. Model-calculated co-tidal (solid line) and co-range (dashed line) charts of (a) M_2 (b) and K_1 tides.

where $V_{\text{monthly mean current}}$ is monthly transport through the open boundary, as described in Lee *et al.* [10].

Starting from a motionless state, we spun up the model with and without tides for two years to remove initial transients, and used the two-year result to facilitate the following discussion.

III. MODEL CO-TIDAL AND CO-RANGE CHARTS

A number of studies have suggested that two amphidromic points spread in the Bohai Sea and Liaodong Bay, respectively; however, some model experiments failed to reproduce them in the same places because of choosing different model parameters [7]. Therefore, it seems being a measure that appearance of the M_2 amphidromic points in the Bohai Sea and Liaodong Bay indicates whether the model is a successful simulation. According to the suggestion of Guo and Yanagi [7] and Lefevre *et al.* [11], we have adopted the same bed drag coefficient ($C_d = 0.0015$) for all model runs in this study. The modeled sea level fields were harmonically decomposed for each major tidal constituent following the programs provided by Foreman [6], and were obtained with corresponding co-phase and co-range major constituent tides in the East China, Yellow, and Bohai seas. The co-phase and co-range charts were drawn using the results of the harmonic analysis of the 3-D model. Fig. 4 partially shows the calculated co-phase and co-range charts. The 3-D model can reproduce two amphidromic points in the Bohai Sea and its northern reach, Liaodong Bay, and two amphidromic points in the Yellow sea for M_2 tides (in Fig. 4(a)), which are similar to

that of Guo and Yanagi [7], Yanagi *et al.* [25], Lefevre *et al.* [11], Wu *et al.* [24], and especially the model results of Lefevre *et al.* [11]. The results for major semidiurnal tides of Lefevre *et al.* [11] show that, along the China coast in the south of the Changjiang mouth, a number of co-phase lines begin from the south of the Changjiang mouth extending to the latitude of 34°N in the China coast. They do not link to the center of the amphidromic point, which is similar to our model results for M_2 and S_2 . In addition, one amphidromic point appears in the southern Bohai Sea and another point appears in Liaodong Bay, which is inferior to the point in the northern Bohai Sea because of an incomplete amphidromic system, as shown in Fig. 4(a). The modeled M_2 amplitude off the west Korean peninsula and in the front of the Changjiang mouth is large, and resembles the model results of Wu *et al.* [24] and Guo and Yanagi [25]. Our model can also effectively reproduce two amphidromic points for K_1 tides, one of which appears in the south of the Shandong peninsula of the Yellow sea and the other appears in the north of the Shandong peninsula (Fig. 4(b)). Obviously, the development of the major diurnal tides is superior to that of the major semidiurnal tides in co-phase amphidromic systems. In addition to comparing the tidal model results of other investigators, our calculated results are also approximately consistent with the observed data, especially for the amphidromic appearance and magnitude of co-range related to the location. A number of tidal models have targeted the reproduction of the two amphidromic points as a measure of accuracy [7]. Apparently, the target must be met with a sensible, yet often costly choice of parameters, among which the crucial parameters are bed drag coefficient, grid size, and accurate representation of

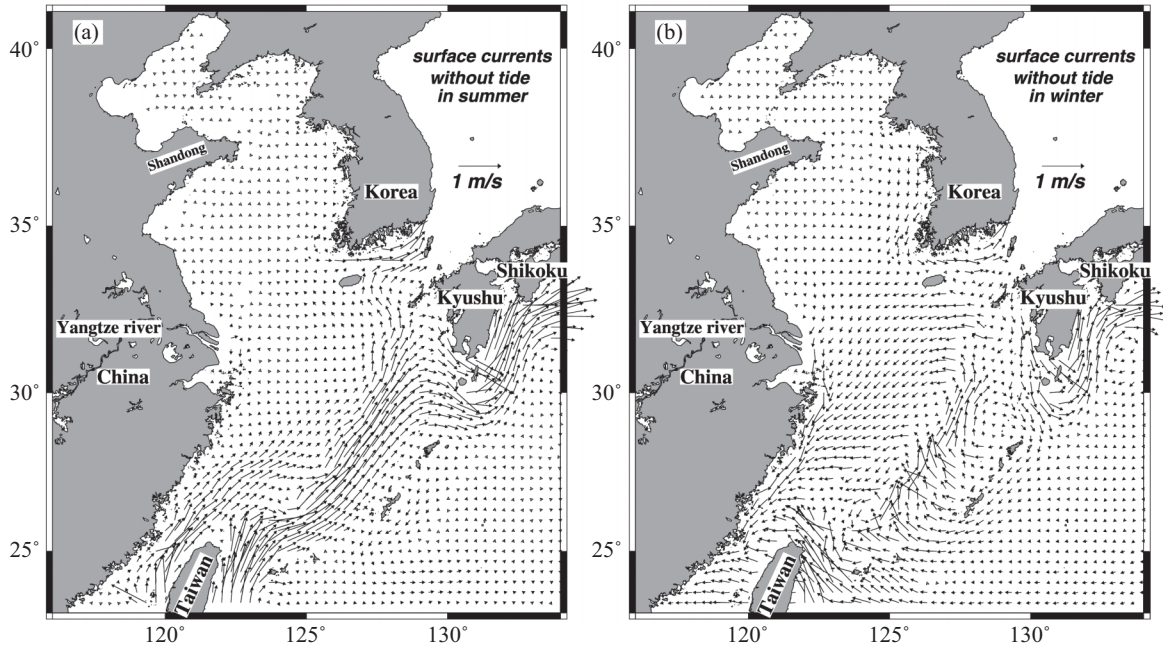


Fig. 5. Model-produced surface flow fields (a) without tides in summer and (b) without tides in winter.

coastline and bottom bathymetry. The following sections present the model results obtained from the tide-circulated coupling model, which was concurrently driven by three forcings, including monthly mean current, tidal forcing, and winds (excluding special announcements in the context).

IV. CIRCULATION FEATURES WITHOUT TIDES

Fig. 5 shows instantaneous snapshots of model-derived circulation at 2.5 m depth in summer (August 30) and winter (December 30) without tides. Without tides, the subtidal summer circulation (Fig. 5(a)) meets our expectations. Off northeast Taiwan, part of the Kuroshio intrudes onto the continental shelf of the East China Sea. The major portion turns from northward to northeastward and thereafter continues to follow the shelf break. The Taiwan Warm Current also enters the East China Sea from the Taiwan Strait and turns eastward to join the main stream of the Kuroshio at approximately 28°N. The summer subtidal circulation in the Yellow and Bohai Seas is weak; hence, it does not obviously affect the Changjiang plume dispersal (Fig. 5(a)).

The subtidal circulation in winter (Fig. 5(b)) also meets the collective past expectations [3, 19]. The on-shelf Kuroshio intrusion off northeast Taiwan becomes more pronounced under the northeast monsoon. The winter monsoon also blocks the northward Taiwan Warm Current from the Taiwan Strait and produces a narrow band of southwestward China Coastal Current from the Changjiang mouth to the Taiwan Strait. Farther north in the Yellow and Bohai Seas, the winter subtidal circulation also weakens with distance away from the East China Sea.

V. INTRA-TIDAL CIRCULATION VARIATION

Fig. 6 shows arbitrarily instantaneous snapshots of model-derived circulation with tides at 2.5 m in depth on August 1 at the 6th, 12th, 16th and 22nd hour of the day. Obviously, tides enrich the shelf circulation. Contemporaneous snapshots show more energized circulation in the East China, Yellow, and Bohai Seas, especially around the mouth of the Changjiang River. In the East China, Yellow, and Bohai seas, the current imposed by tide forcing seems to be stronger than that without tides. Tide-induced shelf currents are as strong as those near the western boundary currents near the ocean surface. The convergent and divergent currents along the coasts are crucial flows for transporting water mass away from the coastal boundaries. The convergent and divergent currents exhibit a radial structure around the region of the Changjiang mouth and influence the Changjiang plume dispersal.

The tide-enhanced circulation is illustrated within a diurnal period. Without an unexpected status as mentioned above, tidal currents near the mouth of the Changjiang River are very strong and exhibit convergent/divergent flow fields [7, 11]. Tidal currents are also notably strong in the Taiwan Strait, along the stretch of China coastline from Changjiang mouth southward, in the northern stretch of the East China Sea bordering Changjiang, and in the Yellow and Bohai Seas. Lefevre *et al.* [11] indicated that tidal elevations can reach 3 m in the Hanchow Bay (near the Changjiang mouth), 3.7 m in the Bohai Bay, 8.5 m in the Incheon Bay (western Korean peninsula), and approximately 5.6 m in the western middle coast of Taiwan (near Chang Hua, 150 km from Taipei). The corresponding tidal currents must be large values; for example, the highest velocities at the inlet/outlet of a bay are more than

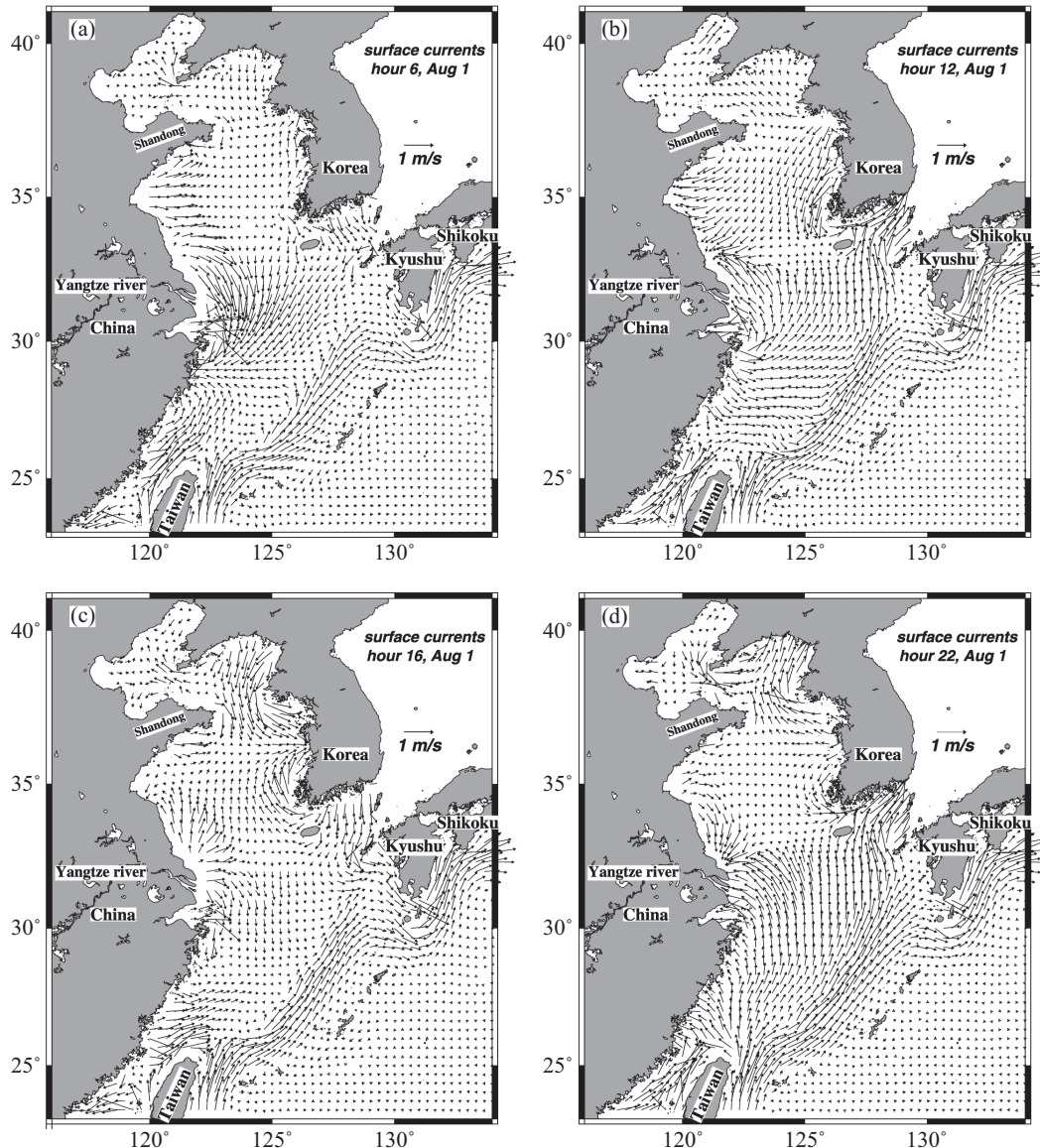


Fig. 6. Model-produced surface flow fields with tides at (a) 6th, (b) 12th, (c) 16th, and (d) 22nd hour on August 1.

3 m/s during ebb tides off the west Korean peninsula. Furthermore, tidal currents converge and diverge twice daily in the northern reaches of the Taiwan Strait and beyond, which is supported by observations [8]. Similar alternating convergence and divergence also occur twice daily between 27°N and 33°N, and off the west Korean peninsula. In addition, corresponding winter features are similar (Figure not shown); however, they differ slightly in strength because of changes in stratification and wind stress.

VI. SURFACE TEMPERATURE FEATURES WITH AND WITHOUT TIDES

Fig. 7 shows instantaneous snapshots of model-derived surface temperature fields at 2.5 m in depth in summer and winter

with and without tides. Figs. 7(a) and 7(b) show model-derived surface temperature fields in summer and winter, respectively, without tides. The overall patterns of the seasonally changing temperature fields in the three-sea system are captured. In the northern reaches (including the Bohai and Yellow Seas), the model-derived SST is almost uniform everywhere, centered at approximately 22°C in summer, and is distributed with quasi-zonal contours that show the cooling source supply from the northern Bohai Sea in winter (Fig. 7(b)). Both plots manifest upward concave contours off the Korean peninsula, which shows a relative cold front flowing southward along the coast. The strongest north-south temperature front always appears between the Changjiang mouth and Tsushima straits, centered at approximately 31°N in summer and winter. In winter, the model to some extent

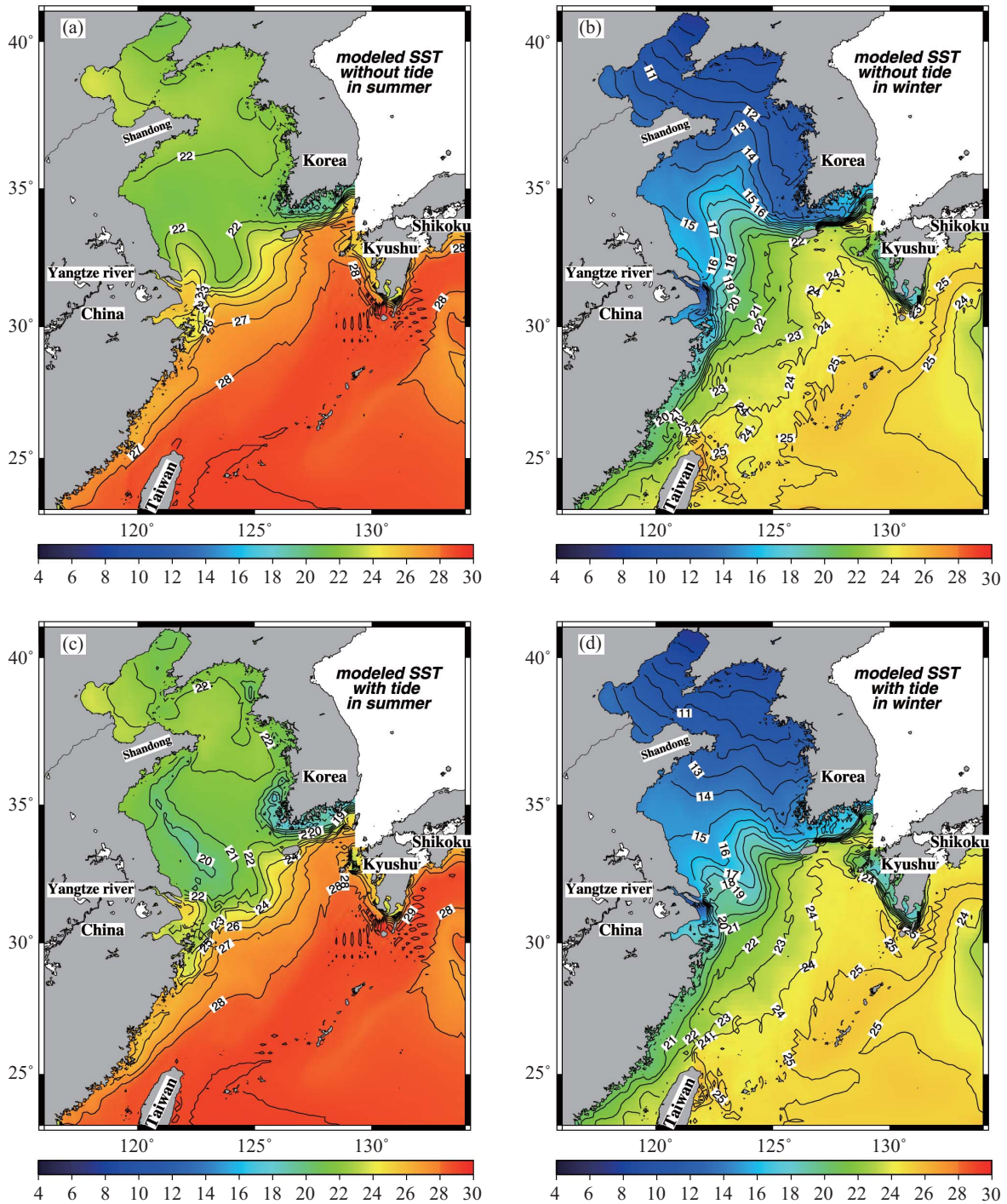


Fig. 7. Model-produced sea-surface temperature (°C) (a) without tides in summer, (b) without tides in winter, (c) with tides in summer, and (d) with tides in winter.

reproduces a meander front stretching from the Changjiang mouth to the southern tip of the Korean Peninsula. Fig. 8 shows the AVHRR image in December, indicating a double-crest structure along the meander front separated by a southward-intruding trough between the Changjiang mouth to the southern tip of the Korean Peninsula. However, in winter, the two meander crests become one in the model without tides.

The AVHRR (The Advanced Very High Resolution Radiometer) image also indicates the southward intrusion of cold water from the Changjiang River along the China coast in winter. The model also reproduced a narrow-band cold-water intrusion southward along the China coastline because of the prevailing northeasterly winds. Figs. 7(c) and 7(d) show the model-derived surface temperature fields in summer and winter,

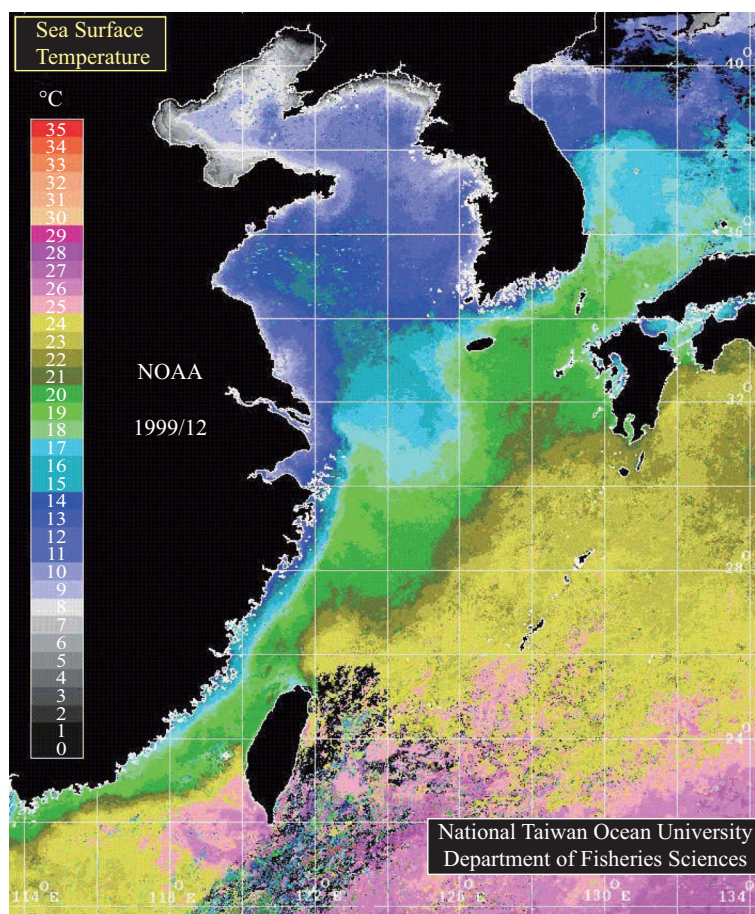


Fig. 8. Winter sea surface temperature derived from NOAA satellite image data. This image is after Lee *et al.* [10].

respectively, with tides. Generally, the temperature distribution with tides is seemingly similar to that of the case without tides in the Yellow and Bohai Seas; however, they exhibit a number of differences in summer and winter. For example, the 22°C contour line turns the coastline of the northern Yellow sea in summer (Fig. 7(c)), and the 20–21°C isothermal lines are distributed from the south of the Shandong Peninsula to the Changjiang mouth along the China coastline. The Changjiang warm tongue is diffused northward and visibly diminished (Fig. 7(c)). In winter, similar to the AVHRR observed data, the model successfully reproduces two meander crests stretching from the Changjiang mouth to the southern tip of the Korean Peninsula, as shown in Fig. 7(d). By comparison, the model results with tides lead to the cold water propagated more south than that without tides.

VII. SURFACE SALINITY FEATURES WITH AND WITHOUT TIDES

Fig. 9 shows instantaneous plots of model-derived surface salinity fields at 2.5 m in depth in summer and winter with and without tides. The model-derived SSS fields capture major features revealed from observations [10] in summer and winter.

In the summer setting, the generally northward current over the shelf suppresses southward expansion without tides. The Changjiang diluted water disperses mainly to the northeast. Fig. 9(a) shows that the balloon-shaped Changjiang plume in summer expands from the river mouth to the northeast. Some of the low salinity waters being transported towards the northeast leave the ECS into the Sea of Japan through the Tsushima straits. For example, the 32 psu isohaline is stretched from the outskirts of the plume to the straits. Another noteworthy feature in summer is the formation of a narrow band of higher salinity in the south of the river mouth along the China coastline. In winter, it is revealed that the Changjiang diluted water (CDW) is visibly disappeared or compressed at the vicinity of the mouth (Fig. 9(b)). Most of the low salinity waters can be carried by the so-called China Coastal Current (CCC) along the southeastern China coast from its mouth into the Taiwan Strait. Some of the CDW in the north of the Changjiang mouth is the remnant from the preceding summer [10]. The north-northeast monsoon forces the low salinity water to intrude southwestward as a narrow band hugging the China coastline.

With tides, Figs. 9(c) and 9(d) show instantaneous plots of the model-derived surface salinity fields at 2.5 m in depth in

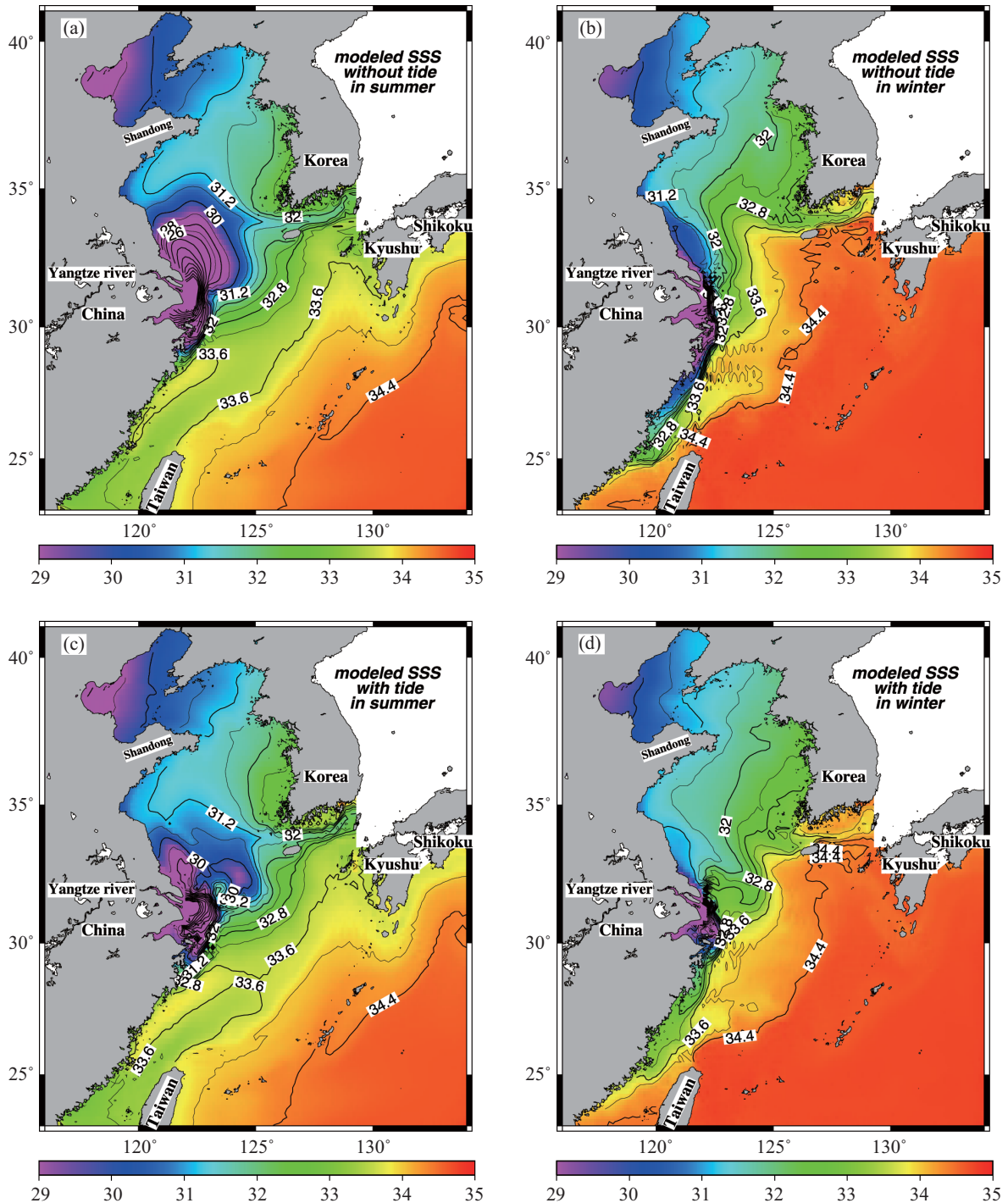


Fig. 9. Model-produced sea-surface salinity (psu) (a) without tides in summer, (b) without tides in winter, (c) with tides in summer, and (d) with tides in winter.

summer and winter, respectively. Excluding similarities, tidal currents generally enhance southward excursion of the CDW plume, regardless of seasons. For example, in summer (Fig. 9(c)), tidal currents shift the core of the CDW plume to south of Changjiang mouth; therefore, the model result is closer to the observation of Beardsley *et al.* [1] and Moon *et al.* [18].

Specifically, the outskirts of the model plume are very similar to their low salinity region during Survey I (June 10-13, 1980; figure not shown), extending almost 100 km seaward to approximately 50 m isobaths. In fact, a comparison of the tidal plume with the non-tidal plume indicated that the CDW plume with tides, however, becomes smaller and more eastward in

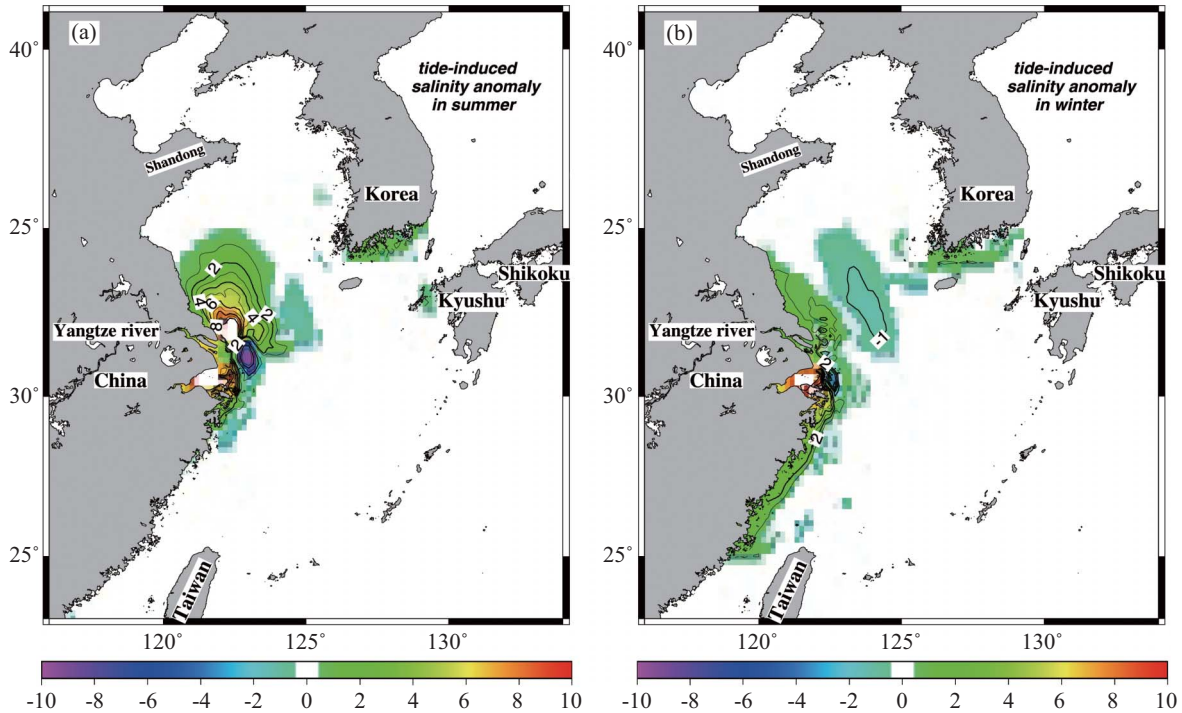


Fig. 10. Tide-induced salinity anomalies at 2.5 m depth in (a) summer and (b) winter.

summer as well as in winter. Therefore, the tidal forcing in this case seems to play a significant role in the processes of horizontal and vertical tidal mixing, especially in the shallow regions. During summer, a small patch of the CDW plume detaches from its major plume and flows towards Cheju Island, as shown in Fig. 9(c). To this point, it had been mentioned in the studies of Moon *et al.* [18] and Lie *et al.* [14]; however, we cannot describe its behavior in detail because of space limitations. In winter, the isohalines are generally oriented in the southwest-northeast direction in the Yellow and Bohai Seas, as well as without tides. By comparison, the tidal forcing leads to a salinity meander off the Changjiang mouth (Fig. 9(d)), which is also noteworthy.

Figs. 10(a) and 10(b) show tide-induced CDW plume anomalies in summer and winter by subtracting the subtidal result from that with tides. In summer, the difference between with and without tides shows that the tide-induced salinity anomalies are mostly spread out to the north and slightly to the south of the Changjiang River (Fig. 10(a)). This indicates a southward net shift. In winter (Fig. 10(b)), the tide-induced salinity anomalies forming a narrow band along the China coastline are positive and with a negative small lens to the northeast of the Changjiang mouth. The positive distribution may extend to a large distance along the China coastline from the latitude of 34°N to the middle reaches of the Taiwan Strait. Interestingly, we find that the tide-induced salinity anomalies in winter are nearly symmetric, which differs from those in summer (see Figs. 10(a) and 10(b)). Theoretically, the forcing of a net southward shift in winter must be similar because it

acts on the CDW plume similarly to that in summer. Both in summer and winter have differing dynamics. This occurs because of the varying hydrographic fields, leading to differing physical processes.

VIII. DISCUSSION AND CONCLUSIONS

Based on a previously validated circulation model driven by monthly climatological winds [9], we incorporated tides into it to develop a tide-circulated coupling numerical model to examine their effects on Changjiang plume dispersal. In this study, we compared the differences of flow, temperature, and salinity fields with and without tides using this coupling model. With or without tides, the three-dimensional coupled model captures major circulation features, such as the Kuroshio, the Taiwan Warm Current, and the China Coastal Current. Tidal currents energize the shelf circulation further. In summer and winter, tidal currents consistently disperse the plume somewhat to the south, the model result of which is closer to the observations. By comparing different cases of data in detail, we find that the plume range of the CDW is markedly larger for the case without tides (Figs. 9(a) and 9(b)) than that with tides (Figs. 9(c) and 9(d)), regardless of whether it occurs in summer or winter. In summer, the difference between with and without tides shows that the tide-induced salinity anomalies are mostly spread to the north and slightly to the south of the Changjiang River (Fig. 10(a)). This indicates a southward net shift. In winter, the tide-induced salinity anomalies forming a narrow band along the China coastline

are positive and detached from the major CDW with a negative small lens to the northeast of the Changjiang mouth. The negative salinity anomalies are stretched from the lens to the Tsushima Strait, leaving the East China Sea from the northern shelf of Cheju Island into the Sea of the Japan (Fig. 10(b)). This indicates that the tidal forcing to transport the low-salinity water entering the Sea of the Japan is more helpful than that without tides in winter. The tide-induced salinity anomalies in winter is approximately 2 psu and distributed between the north of the Changjiang estuary and the middle reaches of the Taiwan Strait along the China coast, implying that the tidal currents may cause strong turbulent mixing with their ambient waters, especially close to the coastal boundaries. Hence, the plume range of the CDW dispersal with tides is reduced more substantially than that without tides.

ACKNOWLEDGMENTS

We are especially grateful for the kind help of C.-K. Hu (TORI) and S. Jan (IONTU). Author HJL was sponsored by the National Science Council (Taiwan) under grants NSC-100-2611-M-019-003.

REFERENCES

1. Beardsley, R. C., Limeburner, R., Yu, H., and Cannon, G. A., "Discharge of the Changjiang (Yangtze River) into the East China Sea," *Continental Shelf Research*, Vol. 4, pp. 57-76 (1985).
2. Chao, S. Y., "River-forced estuarine plume," *Journal of Physical Oceanography*, Vol. 18, pp. 72-88 (1988).
3. Chao, S. Y., "Circulation of the East China Sea, a numerical study," *Journal of the Oceanographical Society of Japan*, Vol. 46, pp. 273-295 (1991).
4. Chao, S. Y. and Boicourt, W. C., "Onset of estuarine plumes," *Journal of Physical Oceanography*, Vol. 16, pp. 2137-2149 (1986).
5. Dean, R. G. and Dalrymple, R. A., *Water Wave Mechanics for Engineers and Scientists*, Prentice-Hall, Inc., Englewood Cliffs, N. J., pp. 1-353 (1984).
6. Foreman, M. G. G. and Henry, R. F., *Tidal Analysis Based on High and Low Water Observations*, Pacific Marine Science Report 79-15, Institute of Ocean Sciences, Patricia Bay, Sidney, British Columbia (1979).
7. Guo, X. and Yanagi, T., "Three-dimensional structure of tidal current in the East China Sea and the Yellow Sea," *Journal of Oceanography*, Vol. 54, pp. 651-668 (1998).
8. Hu, C. K., Chiu, C. T., Chen, S. H., Jan, S., and Tseng, Y. H., "Numerical simulation of barotropic tides around Taiwan," *Terrestrial, Atmospheric and Oceanic Sciences*, Vol. 21, No. 1, pp. 71-84 (2010).
9. Lee, H. J. and Chao, S. Y., "A climatological description of circulation in and around the East China Sea," *Deep-Sea Research II*, Vol. 50, pp. 1065-1084 (2003).
10. Lee, H. J., Chao, S. Y., and Liu, K. K., "Effects of reduced Yangtze River discharge on the circulation of surrounding seas," *Terrestrial, Atmospheric and Oceanic Sciences*, Vol. 15, No. 2, pp. 1-23 (2004).
11. Lefevre, F., Provost, C. L., and Lyard, F. H., "How can improve a global ocean tide model at a regional scale: A test on the Yellow Sea and the East China Sea," *Journal of Geophysical Research*, Vol. 105, No. C4, pp. 8707-8725 (2000).
12. Levitus, S. and Boyer, T., *World Ocean Atlas 1994, Volume 4, Temperature*, NOAA Atlas NESDIS 4, U.S. Department of Commerce, Washington, D.C., Retrieved from <http://ingrid.ldgo.columbia.edu/SOURCES/LEVITUS94/>.
13. Lie, H. J. and Cho, C. H., "On the origin of the Tsushima Warm Current," *Journal of Geophysical Research*, Vol. 99, No. C12, pp. 25081-25091 (1994).
14. Lie, H. J., Cho, C. H., Lee, J. H., and Lee, S., "Structure and eastward extension of the Changjiang River plume in the East China Sea," *Journal of Geophysical Research*, Vol. 108, No. C3, 3077, DOI: 10.1029/2001JC001194 (2003).
15. Liu, K. K., Chao, S. Y., Lee, H. J., Gong, G. C., and Teng, Y. C., "Seasonal variation of primary productivity in the East China Sea: a numerical study based on a coupled physical-biogeochemical model," *Deep-Sea Research II*, Vol. 57, pp. 1762-1782 (2009).
16. Liu, K. K., Gong, G. C., Shyu, C. Z., Pai, S. C., Wei, C. L., and Chao, S. Y., "Response of Kuroshio upwelling to the onset of the northeast monsoon in the sea north of Taiwan: Observations and a numerical simulation," *Journal of Geophysical Research*, Vol. 97, pp. 12511-12526 (1992).
17. Milliman, J. D., Shen, H. T., Yang, Z. S., and Mead, R. H., "Transport and deposition of river sediment in the Changjiang estuary and adjacent continental shelf," *Continental Shelf Research*, Vol. 4, pp. 37-45 (1985).
18. Moon, J. H., Hirose, N., Yoon, J. H., and Pang, I. C., "Offshore detachment process of the low-salinity water around Changjiang bank in the East China Sea," *Journal of Physical Oceanography*, Vol. 40, pp. 1035-1053 (2010).
19. Nitani, H., "Beginning of the Kuroshio," in: Stommel, H. and Yoshida, K. (Eds.), *Kuroshio: Physical Aspects of the Japan Current*, University of Washington Press, pp. 129-163 (1972).
20. Oey, L. Y. and Mellor, G. L., "Subtidal variability of estuarine outflow, plume, and coastal current: a model study," *Journal of Physical Oceanography*, Vol. 23, pp. 164-171 (1993).
21. Pacanowski, R. C. and Philander, S. G. H., "Parameterization of vertical mixing in numerical models of tropical ocean," *Journal of Physical Oceanography*, Vol. 11, pp. 1443-1451 (1981).
22. Pugh, D. T., *Tides, Surges and Mean Sea-Level*, John Wiley and Sons, New York, pp. 1-472 (1987).
23. Sarmiento, J. L. and Bryan, K., "An ocean transport model for the North Atlantic," *Journal of Geophysical Research*, Vol. 87, pp. 394-408 (1982).
24. Wu, H., Zhu, J., Shen, J., and Wang, H., "Tidal modulation on the Changjiang River plume in summer," *Journal of Geophysical Research*, Vol. 116, C08017, DOI:10.1029/2011JC007209 (2011).
25. Yanagi, T., Morimoto, A., and Ichikawa, K., "Co-tidal and co-range charts for the East China Sea and the Yellow Sea derived from satellite altimetric data," *Journal of Oceanography*, Vol. 53, pp. 303-309 (1997).
26. Yankovsky, A. E. and Chapman, D. C., "A simple theory for the fate of buoyant coastal discharges," *Journal of Physical Oceanography*, Vol. 27, pp. 1386-1401 (1997).